Impact of Ni and O vacancies on the electronic properties of NiO: A DFT-based study for optoelectronic applications

View Online   Export Citation   CrossMark

F. Bermúdez-Mendoza,[1] [ID] D. J. Ramos-Ramos,[1] [ID] M. Taeño,[2] [ID] G. C. Vásquez,[1] [ID] D. Maestre,[1] [ID]
F. Domínguez-Adame,[1] [ID] B. Méndez,[1] [ID] R. Martínez-Casado,[1] [ID] and E. Díaz[1,a) [ID]

AFFILIATIONS

[1] Departamento de Física de Materiales, Universidad Complutense, 28040 Madrid, Spain
[2] Centre for Cooperative Research on Alternative Energies (CIC energiGUNE), Basque Research and Technology Alliance (BRTA),
  Alava Technology Park, Albert Einstein 48, 01510 Vitoria-Gasteiz, Spain

Note: This paper is part of the Special Topic on Ultrawide Bandgap Semiconductors.
a)Author to whom correspondence should be addressed: elenadg@ucm.es

ABSTRACT

We present a comprehensive investigation of the impact of Ni and O vacancies on the properties of NiO by employing density functional theory (DFT) and comparing the theoretical predictions with experimental cathodoluminescence data. While B3LYP, HSE06, or HSEsol functionals yield results within the experimental range, we chose B3LYP due to its reliable accuracy and lower computational cost compared to the more complex Hartree–Fock exchange treatment. Our analysis highlights the effectiveness of the B3LYP hybrid functional in reproducing both the experimental lattice constant and the bandgap, reflecting the importance of strong correlation effects in transition metal oxides. We explore the vacancy defects of NiO, revealing that Ni vacancies introduce distinct intra bandgap states whose energy levels can be modulated through defect concentration. In contrast, O vacancies exhibit donor-like characteristics, enhancing n-type conductivity. These defects significantly alter local magnetic moments, revealing a complex interplay between spin and charge dynamics. These findings provide valuable insights into defect engineering strategies aimed at optimizing NiO for advanced applications in optoelectronics. This study also contributes to the broader understanding of transition metal oxides, showcasing the utility of advanced DFT techniques in accurately modeling their properties.

I. INTRODUCTION

Oxides with wide and ultra-wide bandgap (WBG and UWBG) are considered key enabling materials in forefront fields of technological research. However, within this family, p-type oxides are extremely scarce, which strongly motivates their study. Nickel oxide (NiO) is an emerging WBG semiconductor with bandgap energy ranging from 3.6 to 5.0 eV,[1–4] which would allow its potential inclusion in the UWBG family and an intrinsic p-type conductivity, making it highly suitable for a variety of advanced technological applications. Its wide bandgap enables excellent performance in optoelectronic devices,[5] such as ultraviolet (UV) photodetectors

and transparent conducting electrodes. Moreover, NiO exhibits outstanding thermal and chemical stability, which is critical for energy storage applications, including lithium-ion batteries and supercapacitors. Its p-type conductivity, mainly due to the inherent Ni deficiency, positions NiO as a key material to achieve bipolar devices in oxide-based optoelectronics and built-in p–n heterojunctions in many cases in combination with other UWBG oxides as, for example, for self-powered deep-UV photodetectors.[6] In addition, this binary transition metal oxide (TMO), with its robust rock-salt crystal structure and antiferromagnetic (AFM) ordering, serves as an exemplary model for studying strongly correlated systems and Mott insulators. However, the electronic band structure of NiO presents

significant theoretical challenges as its wide bandgap cannot be adequately described by traditional band theories. This characteristic has made NiO a pivotal subject for facing challenging theoretical methods and validating advanced computational approaches, including density functional theory (DFT), which seeks to address the complexities of strong electron correlation.[7]

NiO's magnetic properties further enrich its complexity. At its AFM ground state, spins align symmetrically along the crystal plane (111),[8,9] with a Néel temperature of 523 K.[10,11] These AFM properties make NiO a go-to material in ultrafast spintronic devices and next-generation magnetic recording media, among other applications. Although AFM ordering dominates experimentally, computational studies often simplify simulations by assuming a ferromagnetic (FM) state.[12,13] This simplification can introduce discrepancies between computational predictions and experimental observations, underscoring the importance of explicitly incorporating spin dynamics and symmetry breaking effects in the theoretical modeling.[14]

An accurate evaluation of wide bandgap oxides represents a major challenge for standard implementations of DFT.[15] In particular, strongly correlated electron systems, such as TMO's, often pose difficulties related to ground state prediction and bandgap underestimation. In order to overcome these limitations, standard DFT can be improved by including self-interaction corrections and by using more advanced functionals, such as hybrid functionals, among others. Generalized gradient approximation (GGA) functionals often underestimate the bandgap, although the use of hybrid exchange functionals provides a qualitatively correct description of the crystal structure, cohesion energy, and electronic properties for many different materials, particularly for oxides.[16] While more advanced methods such as dynamical mean-field theory can handle strong electronic correlations with high accuracy, they typically require significantly greater computational resources.[17] In contrast, DFT, especially with hybrid functionals, offers a compelling balance between computational cost and predictive power, making it an efficient choice for studying wide bandgap materials such as NiO. The present study systematically evaluates the electronic properties of NiO by using advanced DFT techniques with the focus on various exchange–correlation functionals. The latter are tested with its accuracy to predict the bandgap. B3LYP, which has a hybrid nature combining local density approximations, GGA, and Hartree–Fock exchange, is identified as the most appropriate. Indeed, it manages to capture the strong electron correlations inherent in TMO's such as NiO within a controlled simulation time.[18,19] On the basis of these results, the effects of Ni and O vacancies on the electronic structure are explored by calculating the density of states (DOS) and band structures under different vacancy configurations. Simulations are performed on a 64-atom supercell comprising 32 Ni and 32 O atoms, with one or two atoms of each type removed to introduce vacancies. The spin polarization of spin-up (α) and spin-down (β) electrons is carefully controlled, revealing intriguing symmetries and asymmetries in the electronic properties across FM and AFM ordering leveraging Crystal23, which use Gaussian-type orbital basis sets further to enhance the precision of the results understanding the interplay between magnetism and electronic structure.[20]

In order to complete our study, we also present cathodoluminescence (CL) measurements performed on NiO samples sintered at variable temperatures to support our theoretical predictions and also

gaining a deeper understanding of the bandgap and the presence of defect-related levels in NiO.

The methodological advancements and discoveries presented here also serve as a blueprint for investigating other strongly correlated materials, aiding in the development of accurate and predictive models for complex oxides. By deepening our understanding of the electronic properties and magnetic ordination of NiO, this work establishes a strong foundation for future studies aimed at harnessing the unique characteristics of TMO's for a wide range of technological applications.

II. METHODS

A. Computational methods

The calculations in this study were performed using Crystal23 software, a specialized tool for solid-state systems that employs localized Gaussian-type orbital basis sets to solve the Kohn–Sham equations of DFT.[20] The NiO system was modeled in its rock-salt crystal structure, represented as a $2 \times 2 \times 2$ supercell containing 64 atoms (32 Ni and 32 O atoms), with a unit cell lattice parameter of 4.177 Å, as shown in Table I.[2]

The basis sets for this work were selected from prior NiO benchmarks with the Crystal code:[22–25] a triple-zeta basis with polarization functions for Ni (three functions per orbital to flexibly represent the localized $3d$ states and their anisotropic spin distributions) and a double-zeta basis with polarization functions for O to describe Ni-O bonding. A test using an even larger Ni basis on the Ni-vacancy defect shifted defect-state energies and magnetic moments by less than 0.1 eV, confirming that the adopted basis sets are sufficiently accurate for modeling defect properties in NiO.

A variety of exchange–correlation functionals were considered for comparison. The Heyd–Scuseria–Ernzerhof hybrid functional (HSE06) is a screened hybrid functional that integrates a portion of Hartree–Fock exchange with a screened Coulomb potential, and its variant HISS, incorporates a higher fraction of exact exchange and a longer-range screening.[26] In addition, the HSEsol functional, optimized for solids, was employed.[27] The Perdew–Burke–Ernzerhof (PBE) functional, based on GGA, and its solid optimized version (PBESOL0), were also studied.[28,29] A recently developed meta-GGA functional, r2SCAN, was included for its ability to combine the

TABLE I. Calculated lattice constants a_0 (Å) and bandgap energy (eV) for NiO using various exchange correlation functionals compared to experimental values given at the bottom row.[1,3,4] Among tested approaches, the B3LYP functional was chosen due to its computational efficiency and accuracy.

Functional	a_0	Bandgap
HSE06	4.1695	4.5779
PBE	4.1810	0.9719
PBESOL0	4.1231	5.1753
HISS	4.1523	5.7970
HSEsol	4.1239	4.4543
r²SCAN	4.1535	2.2265
B3LYP	4.2133	4.2955
Experimental	4.17[21]	3.6–5[1–4]

computational efficiency of GGA functionals, with improved accuracy in describing localized electrons, although it does not incorporate exact exchange.[7,30] The Becke, three-parameter, Lee–Yang–Parr (B3LYP) hybrid functional, identified as the most efficient for this study, blends Hartree–Fock exchange with gradient-corrected correlation terms and was chosen due to its computational efficiency and ability to capture electronic correlation effects, reducing self-interaction errors.[18] Structural optimization of the lattice parameters and internal atomic coordinates was carried out with the Broyden–Fletcher–Goldfarb–Shanno algorithm. Convergence was monitored through the root mean square (rms) and the largest absolute component of the forces. The thresholds for the maximum absolute component and rms forces (and for the corresponding atomic displacements) were set at 0.00045 and 0.00030 a.u. (0.00180 and 0.00120 a.u.), respectively. The optimization was terminated only when all four criteria were satisfied simultaneously. For each defective structure, full relaxation of every atomic position was performed ensuring that local lattice distortions, including Jahn–Teller-type effects, were fully captured. These optimizations used the tighter force threshold of 0.00030 Hartree Bohr^{-1}. The relaxed geometries exhibited localized rearrangements in the vicinity of defect sites, most notably around Ni vacancies.

The self-consistent field (SCF) convergence was enforced with a tight electronic energy of 10^{-7} Hartree, and 6×6 Monkhorst–Pack k-point mesh ensured adequate sampling of the Brillouin zone.[31,32] To explore the AFM ground state of NiO, Fig. 1(a) represents the assignation of the initial spin projections on the Ni sites in a pattern consistent with the AFM-II structure, ensuring an alternating spin-up/spin-down along the (111) crystallographic direction.[9] This approach allows us to carry out a direct comparison between AFM and FM models.[33] The geometry optimization was performed, allowing the system to fully relax and settle at energy minimized geometry. SCF convergence was achieved within 100 cycles with a mixing value of 30% to control the fraction of the new Fock matrix, ensuring stable and well converged electronic densities.

Atomic vacancies were systematically introduced into the NiO supercell to investigate their impact on the optoelectronic properties of the material, as illustrated in Fig. 1(b). First, we created a single Ni vacancy (I) with a spin-up orientation. Next, we added a second single Ni vacancy (II) with a spin-down orientation. We then examined the supercell containing both vacancies (I) and (II). Finally, to probe the effect of different spin alignments, we replaced vacancy (II) with a third vacancy also spin-up (III) and studied the combination (I) and (III). Regarding stability, no difference in energy has been found in the case of a Ni monovacancy for the chosen spin orientations. When two Ni vacancies are introduced into the compound, it is more favorable (by 0.13 eV) if both have the same spin. For our system of 32 Ni atoms, creating a single vacancy corresponds to a 3.125% vacancy concentration, whereas creating two vacancies corresponds to a 6.25%. This approach sheds light on how the interplay between atomic vacancies and magnetic ordering influences the electron charge density distribution (ECHD), spin density (SD) distribution, and ultimately, the overall properties of NiO. Despite oxygen vacancies being less studied in NiO, we also included a single O vacancy (I) to explore how oxygen deficiency can influence the material's properties. The computational parameters for simulations involving vacancies were maintained identical to those used for pristine NiO.

B. Experimental techniques

NiO samples were fabricated using metallic Ni powders (Sigma-Aldrich 99.99%) as precursor material following thermal treatments at temperatures ranging from 800 to 1400 °C under a controlled Ar flow, as described in Ref. 21. Cathodoluminescence analysis was performed in a Hitachi S2500 scanning electron microscope (SEM) at 110 K, using a Hamamatsu PMA-11 CCD detector.

III. RESULTS AND DISCUSSION

A. *Ab-initio* insights into pristine NiO

Table I shows the computed lattice constants a_0 and bandgap energies of NiO using several widely adopted density functionals. Our results highlight the sensitivity of electronic and structural properties of NiO to the chosen exchange correlation functional, usually related to the strong electronic correlations present in this oxide. While standard semilocal functionals (e.g., PBE) underestimate the bandgap for semiconductors, hybrid functionals yield bandgaps within or near the common experimental range (3.6–5.0 eV). For practical comparison, we adopt this widely quoted range while acknowledging that surface effects and possible defects can also significantly impact the measured gap.[1–4,34,35] Notably, B3LYP, HSE06, and HSEsol offer good agreement with experiment, both for the lattice constant and the bandgap.
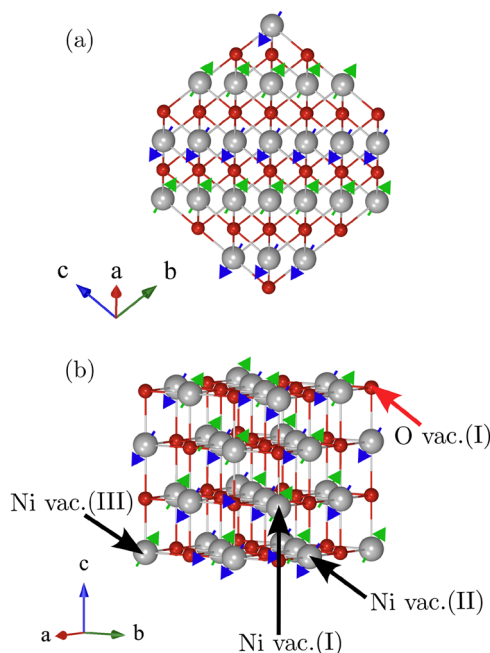
FIG. 1. (a) Schematic representation of the (111) plane of the NiO crystal structure, with Ni atoms depicted in gray and O atoms in red. The green and blue arrows indicate spin-up and spin-down projections, respectively, illustrating the AFM ordering. (b) Illustration of a NiO $2 \times 2 \times 2$ supercell, in which atomic vacancies are introduced: the black arrows indicate the chosen positions of Ni vacancies and the red arrow indicates the chosen position of O vacancy.

Figure 2 shows the spin-polarized density of states (DOS) for NiO calculated using three different exchange–correlation functionals: HSE06, HSEsol, and B3LYP. In all cases, the AFM ground state produces symmetric spin-up and spin-down DOS curves, reflecting the chosen magnetic ordering.[12,13] The partial DOS plots reveal that the bottom of the conduction band primarily consists of Ni $3d$ orbitals, illustrating the charge transfer nature of NiO. Although HSE06, HSEsol, and B3LYP provide results in agreement with experiments (3.6–5.0 eV), we will choose the B3LYP functional hereafter since HSE includes a more sophisticated treatment of Hartree–Fock exchange, making it more computationally expensive.[24,36–38]

## B. Defect engineering of NiO by charge and spin density mapping

Intrinsic defects, such as Ni and O vacancies, play a pivotal role in shaping the electronic, magnetic, and optical properties of NiO.

Although defect-free NiO is a WBG semiconductor with high electrical resistivity, the introduction of defects modifies its electronic and optical properties due to the arising of intra-gap electronic states.[39] For example, Ni vacancies not only play a key role in the p-type conductivity but also significantly alter the electronic structure by creating intra-gap states below the conduction band, while O vacancies affect states close to both the valence and the conduction band. The latter modify the DOS, influence magnetic characteristics, and contribute to emissions observed in luminescence spectra.[21,40]

To gain a deeper insight into the interplay between local defects and electronic and magnetic structure of NiO, we examined electron charge density and spin density maps under certain vacancy configurations; see Fig. 3. In the absence of vacancies, NiO adopts the well-known rock-salt structure characterized by AFM ordered Ni sites.[41,42] The calculated electron charge density clearly shows charge localization around both Ni and O sites, as shown in Fig. 3(a), indicative of the strong ionic and covalent contributions inherent to this TMO.[43]
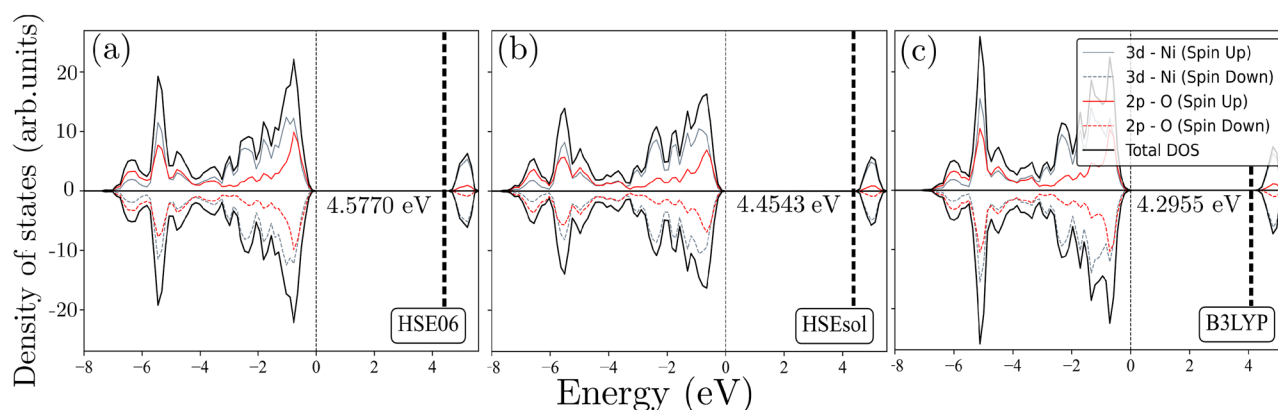
FIG. 2. Density of states (DOS) calculated for NiO using three different functionals: (a) HSE06,[26] (b) HSEsol,[27] and (c) B3LYP.[24,36–38] The thin dashed line indicates the Fermi energy set as the origin of energies, while the wide dashed line indicates the bottom of the conduction band. These plots show the contributions of Ni $3d$-orbitals and the O $2p$-orbitals, considering spin-up and spin-down components. The symmetry in the spin polarized DOS reflects the chosen AFM configuration of the system. Among the three functionals, the B3LYP functional provides an accurate bandgap energy (4.2955 eV) compared to the experimental data within the best computational efficiency.[1–4,34,35]
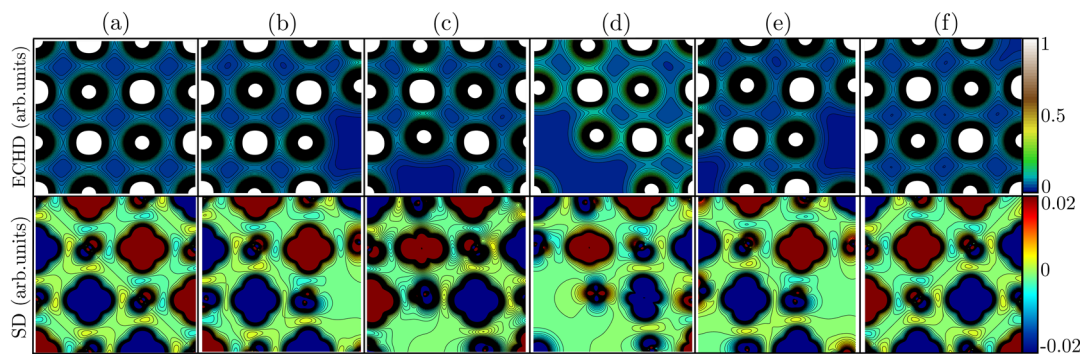
FIG. 3. Electron charge density (ECHD) and spin density (SD) maps for the NiO supercell with different vacancy configurations: (a) ristine NiO, (b) NiO with a single Ni spin-up vacancy (I), (c) NiO with a single Ni spin-down vacancy (II), (d) NiO with two Ni vacancies of spin-up and spin-down projections (I & II), (e) NiO with two Ni vacancies, both of spin-up projection (I & III), and (f) NiO with a single O vacancy (I). The ECHD maps use a color scale where white represents the highest value, while the SD maps use red to indicate spin-up and blue to indicate spin-down. These maps correspond to the faces (100) and (010), in the supercell structure.

All defective supercells were fully relaxed with the hybrid B3LYP functional, allowing the lattice and local spin densities to adjust naturally so that the characteristic atomic distortions and spin-redistribution around isolated vacancies could emerge without bias.[44,45] Optimizing the bulk cell for both the well-established type-II antiferromagnetic (AFM) ground state and two representative ferromagnetic (FM) orderings yielded cubic lattice constants of 4.213 (Å) (AFM) and 4.231 (Å) (FM). Such a difference of only 0.43% and independent checks showed that this <1% volume change alters vacancy-formation energies and magnetic moments by less than 0.01 eV, justifying adoption of the AFM lattice for all defect calculations. Finally, by keeping the vacancy concentration deliberately low (one or two Ni vacancies and just one for oxygen per supercell), interactions between defects are avoided ensuring that the computed properties reflect intrinsic, vacancy-induced perturbations rather than collective effects.[9,25,46]

Introducing a single Ni vacancy, whether with spin-up or spin-down symmetry, reduces the electron density near the vacancy and induces subtle but noticeable rearrangements in the surrounding atomic magnetic moments [Figs. 3(b) and 3(c)]. This rearrangement is accompanied by the emergence of Ni^{3+} states, which promote localized hole formation and significantly affect NiO's overall electronic and magnetic properties.[47] This shift is consistent with previous first-principle investigations illustrating how missing cations in NiO can modify local superexchange interactions.[48] When two Ni vacancies are introduced simultaneously, the spin distribution of the system becomes even more complex. Vacancies with opposite spins Ni (I) & (II) [Fig. 3(d)] create pronounced distortions in neighboring Ni sites spin alignments, whereas Ni (I) & (III) with parallel spins vacancies [Fig. 3(e)] tend to preserve a semblance of the overall AFM pattern. On the contrary, the O (I) vacancy, shown in Fig. 3(f), does not have a significant contribution nor in electron charge or the spin density. These results allow us to achieve a comprehensive perspective on how each type of vacancy influences the delicate balance between charge transfer and magnetic ordering, and they provide valuable guidelines for controlling the properties of NiO through targeted defect manipulation.

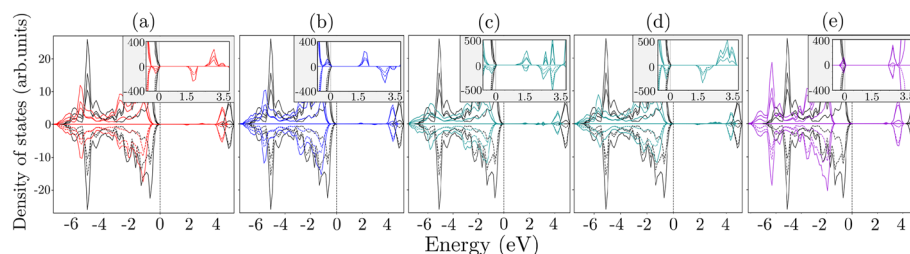## C. Density of states: analysis of vacancy configurations in NiO

As expected, the DOS calculations also reveal significant changes in the electronic structure due to the introduction of

vacancies.[49] In the case of a single Ni vacancy, as shown in Figs. 4(a) and 4(b), localized states emerge within the bandgap. These states are associated with the disruption of the periodic potential and the unpaired electrons resulting from the removal of a Ni atom. The resulting partial filling of the gap indicates a potential for localized intra-gap electronic states to participate in conduction processes under suitable conditions. Furthermore, when comparing the spin-up channel in Fig. 4(a) with the "up-up" combination observed in Fig. 4(d), there appears to be a noticeable increase in the DOS at the same energy levels. This suggests a constructive interaction between the states induced by multiple Ni vacancies, where the overlapping contributions from two vacancies enhance the defect-mediated states and may facilitate conduction through hopping mechanisms, in agreement with the characteristic p-type conductivity experimentally reported for NiO.[11] When two Ni vacancies with different spin orientations (up and down) were introduced, as shown in Fig. 4(c), distinct vacancy-induced states emerge at different energy levels within the bandgap. The separation of these states indicates that the spin degree of freedom influences the energy distribution of the defect states, potentially leading to spin-dependent conduction mechanisms or different contributions to the electronic transport properties.

In contrast, the introduction of an O vacancy, as shown in Fig. 4(e), presents a distinct effect on the electronic structure. The upward shift of the valence band edge toward the Fermi level and the emergence of states in the conduction band region reflect the n-type nature of the defect. This behavior aligns with the expected donor-like character of oxygen vacancies in NiO, where the absence of oxygen results in unoccupied states in the oxygen sub-lattice. These unoccupied states are effectively compensated by electrons, contributing to the conduction band and enhancing electron conductivity. Such n-type behavior[50,51] corroborates experimental and theoretical predictions of donor defect mechanisms in TMO's.[35,52]

D. Band structure analysis of vacancy configurations in NiO

The band structure calculations presented in Fig. 5 provide a detailed understanding of the impact of vacancy defects on the electronic and magnetic properties of NiO. For the pristine NiO structure, represented by the black dashed lines, the calculated bandgap is ~4.2955 eV, which is consistent with the characteristic UV bandgap of undoped NiO ~ (4–4.5) eV,[3,21,53,54] and it agrees

FIG. 4. Density of states (DOS) of NiO with different vacancy configurations, compared to pristine NiO (black lines). (a) One Ni vacancy (I), (b) one Ni vacancy (II), (c) two Ni vacancies (I & II), (d) two Ni vacancies (I & III), and (e) one O vacancy (I). Fermi energy is set as the origin of energies. These plots illustrate the electronic states introduced by the vacancies, and the insets show an enlarged view of the bandgap region to highlight the presence of intermediate states. These states reveal how different vacancy types and configurations modify the electronic structure of NiO.
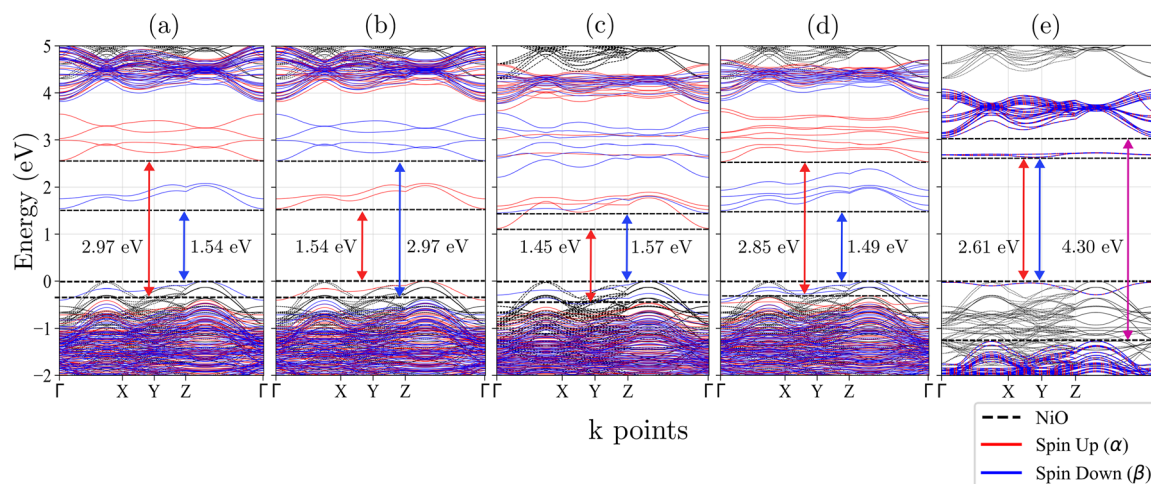
FIG. 5. Band structures of NiO with various vacancy configurations: (a) one Ni vacancy (I), (b) one Ni vacancy (II), (c) two Ni vacancies (I & II), (d) two Ni vacancies (I & III), and (e) one O vacancy (I). The black dashed lines represent pristine NiO band structure. The red lines depict the spin-up (α) channel, and the blue lines represent the spin-down (β) channel. The introduction of vacancies modifies the band structure creating spin polarized states that change the electronic and optoelectronic properties. The presence of intermediate states in the bandgap and spin dependent dispersion highlights the impact of defects on the material's behavior. The k-point path includes high symmetry Γ, X, Y, and Z positions.

perfectly with the data shown in Fig. 5. However, the introduction of Ni and O vacancies causes a reduction in the bandgap, with defect-induced spin-polarized states appearing within the gap. The spin-up (α) states are represented by the red lines, while the spin-down (β) states are depicted in blue, highlighting the differentiation in the bandgap for each spin channel.[5,21]

In Figs. 5(a) and 5(b), we show that the occurrence of a single Ni vacancy, either vacancy (I) or vacancy (II), breaks the symmetry and yields localized spin-polarized states, with computed bandgaps of 2.97 and 1.54 eV, respectively. Notably, if we introduce the vacancy in a spin-up configuration (I) versus a spin-down configuration (II), the resulting bands for each spin channel (α) and (β) interchange, reflecting the symmetry between the two spin channels. Figures 5(c) and 5(d) demonstrate that the introduction of multiple Ni vacancies intensifies the interaction between vacancy states, further reducing the bandgap and increasing the dispersion of the defect bands. In the spin-up/spin-down vacancy configuration shown in Fig. 5(c), we obtain the lowest bandgaps, namely, 1.45 eV for the (α) channel and 1.57 eV for the (β) channel, indicating that opposite spin vacancies lead to pronounced distortions of the spin alignments of neighboring Ni sites. When both vacancies are spin-up, the resulting bandgaps are 2.85 eV for (α) and 1.49 eV for (β), as shown in Fig. 5(d). These findings are reminiscent of introducing a single spin-up vacancy but, due to additional localized states, the bandgap reduces respect to the single vacancy case.

For the case of an O vacancy, Fig. 5(e) shows a distinct shift in the band structure, with defect states emerging closer to the minimum of the conduction band. Unlike Ni vacancies, this configuration does not introduce spin polarization, resulting in a bandgap of 2.61 eV for both (α) and (β) channels. Such donor-like behavior aligns with the n-type conductivity commonly observed in O-deficient NiO.[35,50–52] Defect-related bands fall into lower energy

often overlapping with the near infrared (NIR) and visible regions compared to stoichiometry NiO gap, which remains in the UV range. As the vacancy concentration increases (from 3.1% to 6.3% in our simulations), these defects states progressively shift the absorption edge from the UV toward the visible and even the NIR region.

In line with these observations, experimental data based on luminescence analysis commonly report emissions involving energy levels owing to the variable structure of defects in NiO;[21,40] therefore, luminescence results can provide valuable information to be combined with theoretical calculations.

E. Cathodoluminescence

Luminescence experiments have been commonly employed for the study of semiconducting oxides, including TMOs.[55] Contrary to photoluminescence (PL), in which emission range is restricted by the wavelength of the excitation source, cathodoluminescence (CL), generated by irradiation of electrons with energy of several keV, allows for the study of a wide range of emissions from the probed material, which is particularly relevant for wide bandgap materials. However, CL studies of NiO still remain scarce despite the potential of the technique.[21] Figure 6 shows CL spectra from NiO samples sintered at variable temperatures, ranging from 800 to 1400 °C, where emissions from the near-infrared (NIR) to the UV range can be observed. Gaussian deconvolution of the CL signal, shown in the supplementary material, confirms the presence of emissions centered at around 1.4, 2.0, 2.2–2.5, 3.5, and 4.4 eV. The broad emission in the UV region centered at ~4.4 eV is attributed to near band-edge emissions.[21,54] Such experimental evidence is consistent with our *ab initio* hybrid functional calculations, remarkably, this agrees with B3LYP, which predicts a NiO bandgap close to

22 September 2025 05:41:33
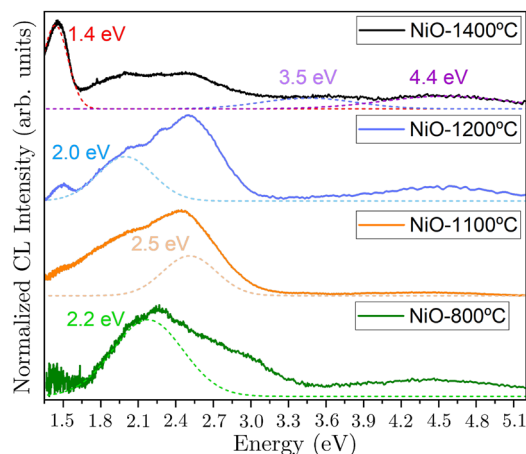
FIG. 6. Cathodoluminescence (CL) spectra obtained from NiO samples sintered at temperatures of 800, 1100, 1200, and 1400 °C. Emission peaks ranging from the near-infrared through the visible to the ultraviolet region are clearly observed. The dashed lines are the Gaussian fits where energy values correspond to the center maximum value, and the solid lines correspond to experimental data.

of the experimental measurements underline the robustness of the theory.

IV. CONCLUSIONS

In this work, we have demonstrated the effectiveness of first-principle methods for investigating the electronic and optoelectronic properties of NiO, paying particular attention to the role of intrinsic defects. Cathodoluminescence measurements from NiO have been analyzed as well, in line with the theoretical calculations. By systematically assessing a variety of exchange–correlation functionals, we have shown that hybrid approaches, most notably B3LYP, capture both the experimentally observed lattice constant and the large bandgap of NiO with excellent accuracy, providing good performance. This highlights the importance of treating strong correlation effects in transition-metal oxides and underscores the need for precise electronic structure methods when modeling (ultra) wide bandgap materials for optical applications.

Our results reveal that Ni and O vacancies lead to markedly variations in the DOS aligned with the reported changes in the NiO's optoelectronic response and the luminescence studies. Ni vacancies introduce localized states within the gap, progressively narrowing the optical gap and enabling intra-gap transitions as the vacancy concentration grows. These localized states imply radiative emissions at sub bandgap energies, in the near infrared range, visible, and UV, reported by luminescence techniques,[21] offering a potential route to tailored broader optical absorption or emission in NiO based devices. Despite NiO usually exhibiting p-type conductivity owing to Ni deficiency, O vacancies can act as donor-like defects promoting n-type conductivity. The resultant defect-induced levels can shift the absorption edge and alter luminescence features, as well as other relevant properties. The optical gap and emission spectra could be selectively manipulated, thereby optimizing NiO for specific optoelectronic applications such as UV photodetectors, transparent conducting oxides, and optoelectronic devices, fields in which NiO has been less explored so far.

Overall, our study establishes that an accurate treatment of exchange and correlation is essential to describe NiO's wide bandgap and its strongly correlated character. It further demonstrates how targeted defect engineering can serve as a powerful tool for tailoring optical absorption, emission, and electronic transport in NiO. These insights lay a foundation for designing advanced NiO based optoelectronic devices and offer a framework for exploring similarly complex transition-metal oxides by the control of the interplay between electron correlation and defect formation as a key to achieve desired functional properties.

4.3 eV in pristine samples. On the other hand, defect-related emission bands in the NIR around 1.4 eV and in the visible centered near to 2.5 eV are more complex and strongly influenced by intragap defect states or localized Ni 3d-orbitals introduced by variations in stoichiometry, defects, morphology, and dimensions, which can be promoted during the sintering treatment.[21] Actually, by increasing the annealing temperature up to 1200 °C, complex emissions around 2.0–2.5 eV are promoted, while the relative intensity of the 1.4 eV emission is higher when annealing at 1400 °C. These CL emissions are mainly associated with Ni vacancies, and the variable density of defects occurred in NiO during the annealing process. The apparent bandgap reduction can be attributable to the formation of additional vacancy states identified in CL spectra that give rise to energy transitions in NIR, visible, and UV. This trend matches the theoretical band structure and DFT calculations described in this work, as shown in Fig. 5, where defect states systematically fill the gap and alter the optoelectronic properties. Moreover, the excellent agreement between the UV bandgap in calculations and the experimentally measured bandgap underlines the robustness of the theory. Meanwhile, the apparent reduction of the visible range bandgap with the annealing temperature, experimentally reported, confirms a direct link between defect formation and modifications to the electronic structure. These states give rise to multiple overlapping bands, reflecting the interplay of Ni and O vacancies and other common point defects in TMOs,[56] whose understanding require further analysis.

DFT calculations including exchange–correlation functionals, in particular B3LYP, considered in this work can shed light on the study of the NiO bandgap value and its variation due to non-stoichiometry, which still remains controversial. In addition, the study of the defect-related levels in NiO appeared as intra-gap states, with energies ranging from the NIR to the UV and variable origins associated with either Ni and/or O vacancies, can be enriched by DFT analysis. The agreement between the calculations and some

SUPPLEMENTARY MATERIAL

The supplementary material provides a comprehensive DFT characterization of the electronic properties of NiO in its ferromagnetic ordering to underscore its limitations for accurately reproducing experimental evidences on NiO. Although the more realistic AFM ordering remains the reference for accurately capturing the actual behavior of NiO, FM solutions yield a useful perspective on the spin-dependent electronic structure. In addition, further details

on experimental CL data and the Gaussian deconvolution of CL spectra can be found in the supplementary material as well.

ACKNOWLEDGMENTS

AUTHOR DECLARATIONS

Conflict of Interest

The authors have no conflicts to disclose.

Author Contributions

F. Bermúdez-Mendoza: Formal analysis (equal); Investigation (equal); Writing – original draft (lead). **D. J. Ramos-Ramos**: Investigation (equal); Writing – review & editing (equal). **M. Taeño**: Investigation (equal); Writing – review & editing (equal). **G. C. Vásquez**: Investigation (equal); Writing – review & editing (equal). **D. Maestre**: Funding acquisition (equal); Investigation (equal); Writing – original draft (equal). **F. Domínguez-Adame**: Funding acquisition (equal); Investigation (equal); Writing – review & editing (equal). **B. Méndez**: Funding acquisition (lead); Investigation (equal); Writing – review & editing (equal). **R. Martínez-Casado**: Investigation (lead); Supervision (lead); Writing – original draft (equal). **E. Díaz**: Investigation (lead); Supervision (lead); Writing – original draft (equal).

DATA AVAILABILITY

The data that support the findings of this study are available within the article and its supplementary material.

REFERENCES

[1] K. Baraik, R. Roychowdhury, A. Bose, C. Mukherjee, T. Ganguli, and S. D. Singh, "Investigation of crystalline and band alignment properties of NiO/GaN and $NiO_{0.5}Co_{0.50}$/GaN heterojunctions using synchrotron radiation based techniques," Phys. Scr. **99**, 065951 (2024).

[2] F. Fiévet, P. Germi, F. de Bergevin, and M. Figlarz, "Lattice parameter, microstrains and non-stoichiometry in NiO. Comparison between mosaic microcrystals and quasi-perfect single microcrystals," J. Appl. Crystallogr. **12**, 387–394 (1979).

[3] G. A. Sawatzky and J. W. Allen, "Magnitude and origin of the band gap in NiO," Phys. Rev. Lett. **53**, 2339–2342 (1984).

[4] A. B. Kunz, "Electronic structure of NiO," J. Phys. C: Solid State Phys. **14**, L455 (1981).

[5] V. N. Hegde, "Structural, dielectric, and optoelectronic properties of green synthesized NiO nanoparticles," Mater. Chem. Phys. **333**, 130319 (2025).

[6] X. Tang, Y. Lu, R. Lin, C.-H. Liao, Y. Zhao, K.-H. Li, N. Xiao, H. Cao, W. Babatain, and X. Li, "Flexible self-powered DUV photodetectors with high responsivity utilizing Ga_2O_3/NiO heterostructure on buffered Hastelloy substrates," Appl. Phys. Lett. **122**, 121101 (2023).

[7] M. J. DelloStritto, A. D. Kaplan, J. P. Perdew, and M. L. Klein, "Predicting the properties of NiO with density functional theory: Impact of exchange and correlation approximations and validation of the r^2SCAN functional," APL Mater. **11**, 060702 (2023).

[8] L. Li and Y. Kanai, "Antiferromagnetic structures and electronic energy levels at reconstructed NiO(111) surfaces: A DFT + U study," Phys. Rev. B **91**, 235304 (2015).

[9] Y. Y. Kyuhyun Lee and S. Han, "Identification of ground-state spin ordering in antiferromagnetic transition metal oxides using the Ising model and a genetic algorithm," Sci. Technol. Adv. Mater. **18**, 246–252 (2017).

[10] N. Rinaldi-Montes, P. Gorria, D. Martínez-Blanco, A. B. Fuertes, I. Puente-Orench, L. Olivi, and J. A. Blanco, "Size effects on the Néel temperature of antiferromagnetic NiO nanoparticles," AIP Adv. **6**, 056104 (2016).

[11] H. Hopoğlu, D. Kaya, M. M. Maslov, S. Kaya, İ. Demir, İ. Altuntaş, F. Ungan, M. Akyol, A. Ekicibil, and E. Şenadım Tüzemen, "Investigating the optical, electronic, magnetic properties and DFT of NiO films prepared using RF sputtering with various argon pressures," Phys. B: Condens. Matter. **661**, 414937 (2023).

[12] M. Gandouzi, A. S. Alshammari, M. Bouzidi, Z. R. Khan, M. Mohamed, and T. Ben Nasrallah, "DFT study of structural optoelectronic and thermoelectric properties of CuNiO ferromagnetic alloys," Phys. Scr. **98**, 075936 (2023).

[13] B. Kisan, J. Kumar, S. Padmanapan, and P. Alagarsamy, "Defect induced ferromagnetism in NiO nanocrystals: Insight from experimental and DFT+U study," Physica B **593**, 412319 (2020).

[14] K. Gillmeister, D. Golež, C.-T. Chiang, N. Bittner, Y. Pavlyukh, J. Berakdar, P. Werner, and W. Widdra, "Ultrafast coupled charge and spin dynamics in strongly correlated NiO," Nat. Commun. **11**, 4095 (2020).

[15] J. Gebhardt and C. Elsässer, "DFT with corrections for an efficient and accurate description of strong electron correlations in NiO," J. Condens. Matter Phys. **35**, 205901 (2023).

[16] M. Lorenz, M. S. R. Rao, T. Venkatesan, E. Fortunato, P. Barquinha, R. Branquinho, D. Salgueiro, R. Martins, E. Carlos, A. Liu, F. K. Shan, M. Grundmann, H. Boschker, J. Mukherjee, M. Priyadarshini, N. DasGupta, D. J. Rogers, F. H. Teherani, E. V. Sandana, P. Bove, K. Rietwyk, A. Zaban, A. Veziridis, A. Weidenkaff, M. Muralidhar, M. Murakami, S. Abel, J. Fompeyrine, J. Zuniga-Perez, R. Ramesh, N. A. Spaldin, S. Ostanin, V. Borisov, I. Mertig, V. Lazenka, G. Srinivasan, W. Prellier, M. Uchida, M. Kawasaki, R. Pentcheva, P. Gegenwart, F. M. Granozio, J. Fontcuberta, and N. Pryds, "The 2016 oxide electronic materials and oxide interfaces roadmap," J. Phys. D: Appl. Phys. **49**, 433001 (2016).

[17] S. Mandal, K. Haule, K. M. Rabe, and D. Vanderbilt, "Systematic beyond-DFT study of binary transition metal oxides," npj Comput. Mater. **5**, 115 (2019).

[18] A. D. Becke, "Density-functional thermochemistry. III. The role of exact exchange," J. Chem. Phys. **98**, 5648–5652 (1993).

[19] P. J. Stephens, F. J. Devlin, C. F. Chabalowski, and M. J. Frisch, "Ab initio calculation of vibrational absorption and circular dichroism spectra using density functional force fields," J. Phys. Chem. **98**, 11623–11627 (1994).

[20] A. Erba, J. K. Desmarais, S. Casassa, B. Civalleri, L. Donà, I. J. Bush, B. Searle, L. Maschio, L. Edith-Daga, A. Cossard, C. Ribaldone, E. Ascrizzi, N. L. Marana, J.-P. Flament, and B. Kirtman, "CRYSTAL23: A program for computational solid state physics and chemistry," J. Chem. Theory Comput. **19**, 6891–6932 (2023).

[21] M. Taeño, J. Bartolomé, L. Gregoratti, P. Modrzynski, D. Maestre, and A. Cremades, "Self-organized NiO microcavity arrays fabricated by thermal treatments," Cryst. Growth Des. **20**, 4082–4091 (2020).

[22] D. Vilela Oliveira, J. Laun, M. F. Peintinger, and T. Bredow, "BSSE-correction scheme for consistent Gaussian basis sets of double-and triple-zeta valence with polarization quality for solid-state calculations," J. Comput. Chem. **40**, 2364–2376 (2019).

[23] M. F. Peintinger, D. V. Oliveira, and T. Bredow, "Consistent Gaussian basis sets of triple-zeta valence with polarization quality for solid-state calculations," J. Comput. Chem. **34**, 451–459 (2013).

[24] T. Bredow and A. R. Gerson, "Effect of exchange and correlation on bulk properties of MgO, NiO, and CoO," Phys. Rev. B **61**, 5194–5201 (2000).

[25] M. D. Towler, N. L. Allan, N. M. Harrison, V. R. Saunders, W. C. Mackrodt, and E. Aprà, "*Ab initio* study of MnO and NiO," Phys. Rev. B **50**, 5041–5054 (1994).

[26] J. Heyd, G. E. Scuseria, and M. Ernzerhof, "Hybrid functionals based on a screened Coulomb potential," J. Chem. Phys. **118**, 8207–8215 (2003).

[27] L. Schimka, J. Harl, and G. Kresse, "Improved hybrid functional for solids: The HSEsol functional," J. Chem. Phys. **134**, 024116 (2011).

[28] J. P. Perdew, K. Burke, and M. Ernzerhof, "Generalized gradient approximation made simple," Phys. Rev. Lett. **77**, 3865–3868 (1996).

[29] A. V. Terentjev, L. A. Constantin, and J. M. Pitarke, "Dispersion-corrected PBEsol exchange-correlation functional," Phys. Rev. B **98**, 214108 (2018).

[30] J. W. Furness, A. D. Kaplan, J. Ning, J. P. Perdew, and J. Sun, "Accurate and numerically efficient r^{2}SCAN meta-generalized gradient approximation," J. Phys. Chem. Lett. **11**, 8208–8215 (2020).

[31] H. J. Monkhorst and J. D. Pack, "Special points for Brillouin-zone integrations," Phys. Rev. B **13**, 5188–5192 (1976).

[32] J. D. Pack and H. J. Monkhorst, "'Special points for Brillouin-zone integrations'—A reply," Phys. Rev. B **16**, 1748–1749 (1977).

[33] S. Elmassi, M. Beraich, M. Bousseta, A. El Mouncharih, L. Amiri, S. Drissi, A. Abali, L. Nkhaili, A. Narjis, A. El kissani, A. Alsaad, and A. Outzourhit, "Theoretical and experimental investigations of the effect of cobalt doping on the structural, optical and electrical properties of sputtered NiO films for optoelectronic applications," Opt. Mater. **145**, 114449 (2023).

[34] M. Bonomo, "Synthesis and characterization of NiO nanostructures: A review," J. Nanopart. Res. **20**, 222 (2018).

[35] S. Suman, A. Behra, and P. Swaminathan, "Oxygen-modulated photoresponse in nickel oxide thin films for wide band gap photodetector application," Discover Appl. Sci. **7**, 84 (2025).

[36] C. H. Patterson, "Comparison of hybrid density functional, Hartree–Fock, and GW calculations on NiO," Int. J. Quantum Chem. **106**, 3383–3386 (2006).

[37] J. Muscat, A. Wander, and N. M. Harrison, "On the prediction of band gaps from hybrid functional theory," Chem. Phys. Lett. **342**, 397–401 (2001).

[38] D. S. Middlemiss and W. C. Mackrodt, "First principles study of d → d excitations in bulk NiO," Mol. Phys. **103**, 2513–2525 (2005).

[39] T. M. Schuler, D. L. Ederer, S. Itza-Ortiz, G. T. Woods, T. A. Callcott, and J. C. Woicik, "Character of the insulating state in NiO: A mixture of charge-transfer and Mott–Hubbard character," Phys. Rev. B **71**, 115113 (2005).

[40] A. Gandhi and S. Wu, "Strong deep-level-emission photoluminescence in NiO nanoparticles," Nanomaterials **7**, 231 (2017).

[41] W. J. Meang, J. Seo, Y. Ahn, and J. Y. Son, "Magnetic force microscopy of conducting nanodots in NiO thin films," Electron. Mater. Lett. **12**, 251–254 (2016).

[42] S. D. Tiwari and K. P. Rajeev, "Magnetic properties of NiO nanoparticles," Thin Solid Films **505**, 113–117 (2006).

[43] S. L. Dudarev, G. A. Botton, S. Y. Savrasov, C. J. Humphreys, and A. P. Sutton, "Electron-energy-loss spectra and the structural stability of nickel oxide: An LSDA+U study," Phys. Rev. B **57**, 1505–1509 (1998).

[44] A. M. Ferrari, C. Pisani, F. Cinquini, L. Giordano, and G. Pacchioni, "Cationic and anionic vacancies on the NiO(100) surface: DFT + U and hybrid functional density functional theory calculations," J. Chem. Phys. **127**, 174711 (2007).

[45] J. A. Dawson, Y. Guo, and J. Robertson, "Energetics of intrinsic defects in NiO and the consequences for its resistive random access memory performance," Appl. Phys. Lett. **107**, 122110 (2015).

[46] A. Schrön, C. Rödl, and F. Bechstedt, "Crystalline and magnetic anisotropy of the 3d-transition metal monoxides MnO, FeO, CoO, and NiO," Phys. Rev. B **86**, 115134 (2012).

[47] X. Xu, H. Zhang, Y. Tong, Y. Sun, X. Fang, J. Xu, and X. Wang, "Tuning Ni^{3+} quantity of NiO via doping of cations with varied valence states: The key role of Ni^{3+} on the reactivity," Appl. Surf. Sci. **550**, 149316 (2021).

[48] F. Pielmeier and F. J. Giessibl, "Spin resolution and evidence for superexchange on NiO(001) observed by force microscopy," Phys. Rev. Lett. **110**, 266101 (2013).

[49] K. O. Egbo, C. P. Liu, C. E. Ekuma, and K. M. Yu, "Vacancy defects induced changes in the electronic and optical properties of NiO studied by spectroscopic ellipsometry and first-principles calculations," J. Appl. Phys. **128**, 135705 (2020).

[50] P. Gupta, T. Dutta, S. Mal, and J. Narayan, "Controlled p-type to n-type conductivity transformation in NiO thin films by ultraviolet-laser irradiation," J. Appl. Phys. **111**, 013706 (2012).

[51] R. Molaei, R. Bayati, and J. Narayan, "Crystallographic characteristics and p-type to n-type transition in epitaxial NiO thin film," Cryst. Growth Des. **13**, 5459–5465 (2013).

[52] H. Wang, J. Zhang, and S. Tao, "Nickel oxide nanoparticles with oxygen vacancies for boosting biomass-upgrading," Chem. Eng. J. **444**, 136693 (2022).

[53] H. Moreno Fernández, J. Gallenberger, C. Mempin, I. Khalek, M. Neumann, S. Lotfi, S. M. Kim, M. Li, C. Tian, and J. P. Hofmann, "Phase transitions in NiO during the oxygen evolution reaction assessed via electrochromic phenomena through operando UV–Vis spectroscopy," Electrochim. Acta **498**, 144626 (2024).

[54] W. C. Mackrodt, S. Salustro, B. Civalleri, and R. Dovesi, "Low energy excitations in NiO based on a direct Δ-SCF approach," J. Phys.: Condens. Matter **30**, 495901 (2018).

[55] M. Nyborg, I. Kolevatov, G. C. Vásquez, K. Bergum, and E. Monakhov, "Dominant defects and carrier transport in single crystalline cuprous oxide: A new attribution of optical transitions," J. Appl. Phys. **130**, 175701 (2021).

[56] V. I. Anisimov, I. V. Solovyev, M. A. Korotin, M. T. Czyżyk, and G. A. Sawatzky, "Density-functional theory and NiO photoemission spectra," Phys. Rev. B **48**, 16929–16934 (1993).

22 September 2025 05:41:33